

Article

## Numerical Study of the Simultaneous Oxidation of NO and SO<sub>2</sub> by Ozone

Bo Li <sup>1,2,\*</sup>, Jinyang Zhao <sup>1</sup> and Junfu Lu <sup>2</sup>

<sup>1</sup> Electric Power Planning & Engineering Institute, Ande Rode No. 65, Xicheng District, Beijing 100120, China; E-Mail: jyzhao@cpecc.net

<sup>2</sup> Key Laboratory for Thermal Science and Power Engineering of Ministry of Education, Department of Thermal Engineering, Tsinghua University, Beijing 100083, China; E-Mail: lvjf@mail.tsinghua.edu.cn

\* Author to whom correspondence should be addressed; E-Mail: boli@cpecc.net; Tel.: +86-010-5838-8537; Fax: +86-010-5838-8596.

Academic Editor: Christian Kennes

Received: 29 September 2014 / Accepted: 9 January 2015 / Published: 29 January 2015

---

**Abstract:** This study used two kinetic mechanisms to evaluate the oxidation processes of NO and SO<sub>2</sub> by ozone. The performance of the two models was assessed by comparisons with experimental results from previous studies. The first kinetic mechanism was a combined model developed by the author that consisted of 50 species and 172 reactions. The second mechanism consisted of 23 species and 63 reactions. Simulation results of both of the two models show under predictions compared with experimental data. The results showed that the optimized reaction temperature for NO with O<sub>3</sub> ranged from 100~200 °C. At higher temperatures, O<sub>3</sub> decomposed to O<sub>2</sub> and O, which resulted in a decrease of the NO conversion rate. When the mole ratio of O<sub>3</sub>/NO was greater than 1, products with a higher oxidation state (such as NO<sub>3</sub>, N<sub>2</sub>O<sub>5</sub>) were formed. The reactions between O<sub>3</sub> and SO<sub>2</sub> were weak; as such, it was difficult for O<sub>3</sub> to oxidize SO<sub>2</sub>.

**Keywords:** ozone injection; kinetic modeling; nitrogen oxides; sulfur dioxide; multi-pollutant control technology

---

## 1. Introduction

Air pollution is now one of the most serious environmental problems worldwide. The flue gas of coal-fired power plants usually contains fine particles such as SO<sub>2</sub>, NO<sub>x</sub> and mercury [1,2]. Although China is a country with many coal-fired power plants, emission standards have been strengthened in recent years [3]. Pollution control systems are required in order to meet these newer strict emission regulations. Conventional coal-fired power plants usually combine multiple single pollutant control facilities for emission control purposes. In recent years, various kinds of technologies have been developed to reduce worldwide SO<sub>2</sub> and NO<sub>x</sub> emissions [4–6]. In order to remove SO<sub>2</sub>, several wet desulphurization technologies, including the calcium-gypsum process, magnesium oxide scrubbing and the double alkaline process have been widely applied in coal-fired power plants. Typically, one of these three methods is adopted to achieve NO<sub>x</sub> emission control [7,8]. These methods include Low-NO<sub>x</sub> burner technology (used to reduce the formation of NO<sub>x</sub> in the furnace), Selective Catalytic Reduction (SCR) technology and Selective Non-Catalytic Reduction technology (SNCR).

A multi-pollutant control system is defined as: a system that can remove two or more of the principle regulated pollutants (SO<sub>2</sub>, NO<sub>x</sub> particulate matter, mercury and CO<sub>2</sub>) in a single reactor or a single system designed for control purposes [9]. Numerous simultaneous removal techniques have been previously investigated [10,11], including the dry absorption method [12], the electron beam process [13] and the wet oxidation method [14]. In the wet oxidation method, various oxidation agents are used to oxidize NO<sub>x</sub> and SO<sub>2</sub>, including chlorine dioxide [15], sodium chlorite [16], hydrogen peroxide [17] and ozone [18,19]. As a stable molecule, O<sub>3</sub> is a potentially useful oxidant in practical applications. O<sub>3</sub> is generated in a non-thermal plasma reactor and then injected into the flue gas duct or a NO<sub>x</sub> reactor. NO<sub>x</sub> and SO<sub>2</sub> are then oxidized into higher oxides and mercury is able to be oxidized into mercury oxide. Numerous studies have investigated the O<sub>3</sub> oxidation of flue gas [20–26]. These studies demonstrated that ozone could be an efficient oxidizing agent for the oxidation of NO. Wang *et al.* experimentally investigated the simultaneous removal of NO<sub>x</sub> and SO<sub>2</sub> in the nitrogen flow of a narrow reactor by ozone injection [20]. The results showed that the injection of ozone could simultaneously react with both NO and SO<sub>2</sub>, with NO being oxidized to a higher oxidation state. Also, in this study, the optimal temperature for NO oxidation of 473 K was suggested. Sun *et al.* studied the O<sub>3</sub> oxidation processes of NO and SO<sub>2</sub> using an *in situ* IR spectrometer [21]. Experimental results showed that the O<sub>3</sub> concentration and the reaction temperature played critical roles in the O<sub>3</sub> oxidation process of NO. When the molar ratio of O<sub>3</sub>/NO was greater than 1, the oxidation products were NO<sub>2</sub>, N<sub>2</sub>O<sub>5</sub> and HNO<sub>3</sub>; however, O<sub>3</sub> did not significantly oxidized SO<sub>2</sub> for that this reaction has high energy barrier. Skalska *et al.* investigated the intensification of the NO<sub>x</sub> absorption process by means of ozone injection into the exhaust gas stream; results showed that, due to oxidation, the efficiency of the NO<sub>x</sub> absorption was much higher than without the ozone injection [22], the reason is that NO could be efficiently oxidized by O<sub>3</sub> into NO<sub>2</sub> and other products of higher oxidation state of NO, these products are water-soluble and can be absorbed by alkaline solution. Mok proposed a two-stage process consisting of an ozonizing chamber and an absorber containing a reducing agent solution. The injection of ozone led to rapid oxidation of NO to a higher oxidation state and NO<sub>x</sub> removal was achieved by absorption using sodium sulfide along with the removing of SO<sub>2</sub> [23]. Sun *et al.* studied the simultaneous absorption process of NO<sub>x</sub> and SO<sub>2</sub> from flue gas with a pyrolusite slurry combined with a gas-phase oxidation of NO using ozone [24]. The results

revealed that ozone could oxidized NO to NO<sub>2</sub> with a high degree of efficiency. The MnO<sub>2</sub> in the pyrolusite slurry oxidized SO<sub>2</sub> and NO<sub>2</sub> into MnSO<sub>4</sub> and Mn(NO<sub>3</sub>)<sub>2</sub>, respectively, in the liquid phase.

Due to a lack of kinetic models, previous studies rarely provided a detailed chemical process of NO and SO<sub>2</sub> oxidation by O<sub>3</sub>. As such, the interactions of NO and SO<sub>2</sub> during the oxidation process have not been fully investigated. This paper focuses on the chemical process in its presentation of a detailed study on the kinetic mechanisms of the oxidation of NO and SO<sub>2</sub> by O<sub>3</sub>. Based on the findings, the optimized reaction conditions for the practical application of O<sub>3</sub> injections for multi-pollutant controls in coal-fired power plants are provided. In particular, this study considers two mechanisms in order to evaluate the oxidation process. The performance of the two mechanisms are first assessed by comparisons with experimental data from Mok *et al.* [25] and Stamate *et al.* [26]. The oxidation of NO and SO<sub>2</sub> by O<sub>3</sub> are then discussed by comparisons of simulation results with experimental results from Wang *et al.* [27] (in Chinese) and Wang *et al.* [28] (in Chinese). Next, further insights are provided into the kinetic mechanisms that control the oxidation process of NO and SO<sub>2</sub> with O<sub>3</sub>.

## 2. Experimental Setup

A multi-layers plug-flow quartz reactor was used for the experiment setup [20]. The experiment apparatus consisted of ozone generation, a quartz flow reactor, an O<sub>3</sub> analysis system and an online gas analysis system (Figure 1).

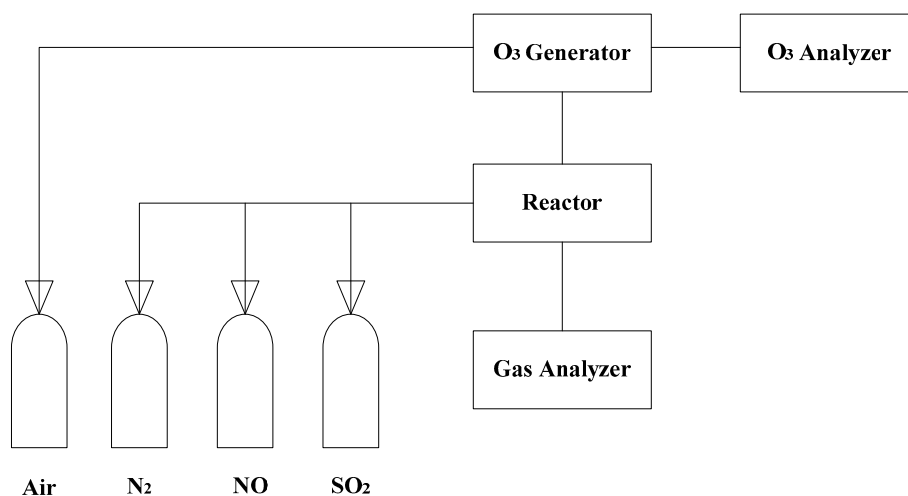


**Figure 1.** Schematic diagram of the experimental apparatus [20].

The oxidation reactions occurred in the quartz flow reactor, as shown in Figure 2. A special delicate flow reactor (with a three-channels homocentric reaction tube) was designed and made by quartz glass in order to reduce the impact of the non-uniform temperature profile of the furnace. The reactor had a total length of 642 mm and an outer-diameter of 20 mm. The heating length of the electric furnace was 600 mm. The reactions occurred in the center tube. The tube had an inside diameter of 5 mm and a length of 100 mm. The center tube was surrounded by O<sub>3</sub>, and the temperatures of O<sub>3</sub> and the mixtures in the center tube were identical, thus it could be considered that there was no heat transfer between the center tube and outside. Therefore, the center tube was treated as an isothermal reactor. The NO/SO<sub>2</sub>/N<sub>2</sub> mixtures entered the reactor through inlet 2 and then passed through a reciprocating preheating channel

before entering the center tube. O<sub>3</sub> was generated in the ozone generator; it then flowed into the reactor through inlet 1 where it was heated by a separate preheating channel. The two well-preheated streams instantly mixed with each other at the nozzle of center tube.

The ozone was generated by a dielectric barrier discharge (DBD) device with 3.7–4 kVAC voltage and 5 kHz (model CF-G-3-010G). The output concentration of O<sub>3</sub> was continuously monitored by an ozone analyzer. The simulated flue gas was prepared by N<sub>2</sub> and small amount of concentrated NO gas and SO<sub>2</sub> gas. Oxygen was not absent in the main flow in these experiments. The flow rate of the gas was all controlled by mass flow controller [20]. The total flow rate of all reactants, including O<sub>3</sub> and simulated flue gas, were fixed to 1000 mL/min. The residence time in the center tube ranged from 0.049–0.089 s and varied with temperature (calculated by 33.3 K/T s).

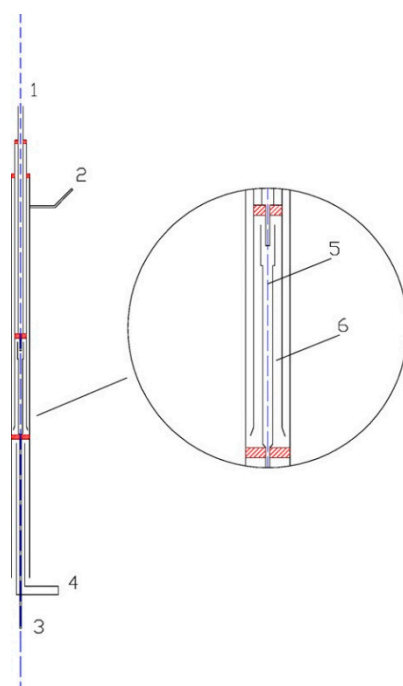


**Figure 2.** Schematic of the quartz flow reactor. (1) Inlet 1; (2) Inlet 2; (3) Outlet; (4) Air cooling; (5) Quartz flow reactor; (6) Preheat channels [20].

### 3. Kinetic Modeling and Numerical Simulation Methodology

#### 3.1. Kinetic Mechanism Description

This study used two kinetic mechanisms to model the oxidation process of NO/O<sub>3</sub>, SO<sub>2</sub>/O<sub>3</sub> and NO/SO<sub>2</sub>/O<sub>3</sub>. The first kinetic mechanism is a combined model developed by the author, consisting of 50 species and 172 reactions (Model I). Model I considered three kinds of reactions: NO/O<sub>3</sub> reactions (referenced in Wen *et al.* [29]); SO<sub>2</sub>/O<sub>3</sub> reactions (referenced in Wang [28]); and NO/SO<sub>2</sub> reactions (referenced online [30]). The second kinetic mechanism was developed by Sun *et al.* [21] based on the situ IR spectrometer measurements. It consisted of 23 species and 63 reactions (Model II). Table 1 shows the key reactions and parameters for Model I and Model II. The key reactions of the two models were identical and the parameters were different. The supplementary file lists the other reactions of the two

models. Most of the reactions of the two models were different. For example, there were 112 reactions to describe the oxidation process of SO<sub>2</sub> and SO<sub>2</sub>/NO in Model I and 8 reactions for Model II.

**Table 1.** Comparisons of parameters for key reactions of Model I and Model II.

Reactions	Model I		Model II	
	A (cm <sup>3</sup> /mol-s)	Ea (cal/mol)	A (cm <sup>3</sup> /mol-s)	Ea (cal/mol)
O <sub>3</sub> + NO = NO <sub>2</sub> + O <sub>2</sub> (R1)	1.8E + 12	2722	8.43E + 11	2605
O <sub>3</sub> + NO <sub>2</sub> = O <sub>2</sub> + NO <sub>3</sub> (R2)	7.22E + 10	4870	8.43E + 10	4913
O <sub>3</sub> + SO <sub>2</sub> = O <sub>2</sub> + SO <sub>3</sub> (R3)	1.81E + 12	13,910	1.81E + 12	13,923
O <sub>3</sub> = O <sub>2</sub> + O (R4)	2.0E + 15	23,250	4.31E + 14	22,277
O <sub>3</sub> + O = O <sub>2</sub> + O <sub>2</sub> (R5)	4.82E + 12	4093	4.82E + 12	4098

Model I is a detailed mechanism in which the three kinds of reactions are validated by experimentation [28–30]. Model II is relatively small and can reduce computational costs when used for predictions. The differences in the reaction parameters may be the result of differences in the reaction paths and, therefore, the prediction results. The following sections address this matter in further detail.

### 3.2. Simulation Strategy

The present kinetic calculations were performed using the Plug Flow Reactor (PFR) computer code [31] which was used to predict the oxidation process of NO/O<sub>3</sub>, SO<sub>2</sub>/O<sub>3</sub> and NO/SO<sub>2</sub>/O<sub>3</sub> in a multi-layers plug-flow quartz reactor. The PFR model was used to describe a suitable steady-state, tube flow reactor for process design, optimization and control. The mixing in the axial flow direction was ignored, but perfect mixing in the directions transverse to this were taken into account for the PFR models. Thermodynamic curve fits were obtained from the National Institute of Standards and Technology chemical species database [32].

The gaseous mixtures were introduced into the PFR at 101.3 kPa. The starting point of the distance was  $x = 0$ . In Section 4.1, the initial NO concentration, the molar ratio of NO/O<sub>3</sub> and the temperature were maintained in accordance with experiments from Mok *et al.* [25] and Stamate *et al.* [26], detailed experimental conditions are introduced in Section 4.1. In Section 4.2 and Section 4.3, the diameter and the length of the PFR reactor were kept at 5 mm and 100 mm. The residence time were ranged from 0.049–0.089 according to different temperatures. In Section 4.1, the initial NO concentration, the molar ratio of NO/O<sub>3</sub> and the temperature were maintained in accordance with experiment [27]. Regard to the discussion of temperature effect on the NO conversion rate, the initial NO concentration was 300 ppm, O<sub>3</sub>/NO mole fraction was 1.0, the residence time was kept at 1 s. Regard to the discussion of the effect of the molar ratio of O<sub>3</sub>/NO on reaction products, the temperatures were kept at 100 °C and 200 °C respectively, the initial NO mole fraction was maintained at 300 ppm, O<sub>3</sub>/NO mole fraction was 1.5 and 2.0, the residence time was kept at 1s. In section 4.3, the initial SO<sub>2</sub> concentration, the molar ratio of SO<sub>2</sub>/O<sub>3</sub> and the temperature were maintained in accordance with experiment [28]. In Section 4.4, the O<sub>3</sub>/NO/SO<sub>2</sub> mole fraction was 2:1:1 and the initial concentration of NO and SO<sub>2</sub> was 300 ppm.

## 4. Results and Discussion

### 4.1. Model Validation

The two kinetic models are first validated with the published experimental results. Figure 3 depicts the comparison of predicted results with the experimental data of NO<sub>2</sub> concentration from Mok *et al.* [25] and Stamate *et al.* [26]. The experiments in Ref. [25] were conducted in an ozonizing chamber. O<sub>3</sub> produced in a DBD device was continuously fed to the ozonizing chamber to convert NO into NO<sub>2</sub>. The exhaust gas was prepared by mixing air and small amounts of concentrated NO gas balanced with N<sub>2</sub>. The residence time was kept at 2.9 s. In Ref. [26], a 4.5 m long and 0.6 m in diameter reactor with a residence time of the flue gas of about 5 s was used to oxidize the NO. NO<sub>2</sub> in the reactor were measured by FTIR. As shown in Figure 3, the numerical simulation results calculated by the two models were lower than those of the experimental results. The NO<sub>2</sub> concentrations first increased and then decreased. Where the molar ratio O<sub>3</sub>/NO equaled 1.0, the concentration of NO<sub>2</sub> reached a maximum value. This is in accordance with previous findings [33]. Skalska *et al.* investigated the mole concentration of products at different O<sub>3</sub>/NO mole fractions experimentally [33], results revealed that if the molar ratio of O<sub>3</sub>/NO is higher than 1.0, NO<sub>2</sub> will react with O<sub>3</sub> and generate higher nitrogen oxides, NO<sub>3</sub>. Also, N<sub>2</sub>O<sub>5</sub> is formed as a result of the reaction of NO<sub>2</sub> with NO<sub>3</sub>. The under-predictions of simulations shown in Figure 3a,b are probably caused by both the experimental uncertainties and the estimation uncertainties of reaction parameters in the reactions of the two kinetic models. More work is necessary to be conducted on the kinetic modeling in the future.

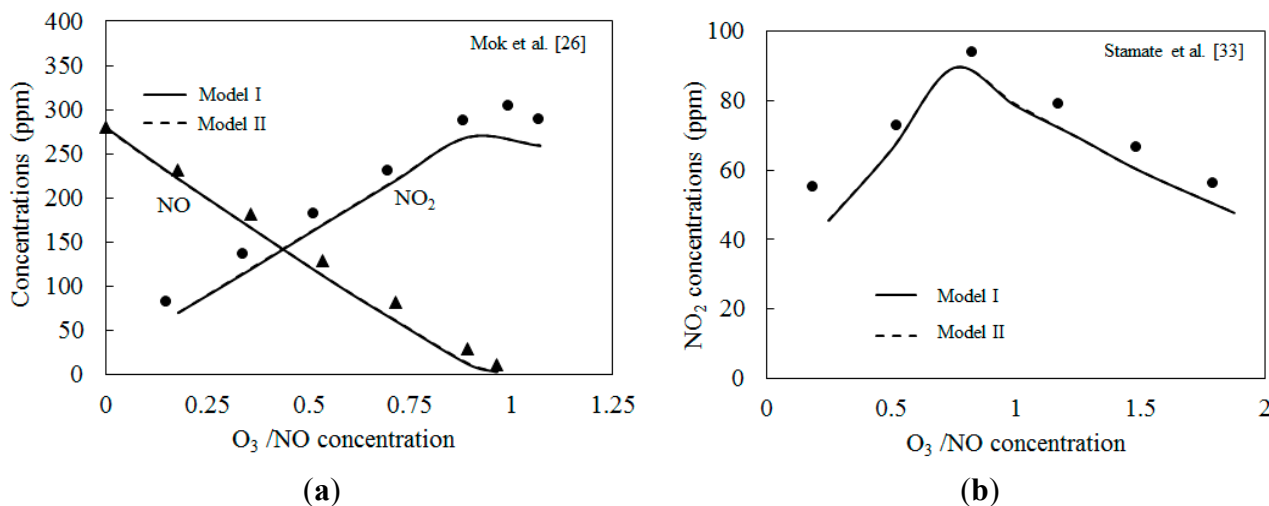


**Figure 3.** Comparison of predicted results with experimental data. (a) Initial NO: 280 ppm, NO<sub>2</sub>: 20 ppm, 25 °C; (b) Initial NO: 80 ppm, 40 °C.

### 4.2. NO Oxidation by O<sub>3</sub>

Figure 4 depicts the concentrations of NO obtained by varying the O<sub>3</sub>/NO concentrations at temperature T = 100 °C. Here, the O<sub>3</sub>/NO concentrations ranged from 0.0 to 1.1. Figure 4 also provides comparisons of the experimental data [27] and simulation results with Model I and Model II. The NO concentration decreased as the O<sub>3</sub>/NO concentrations increased. Where the O<sub>3</sub>/NO concentration was less than 1.0, O<sub>3</sub> reacted with NO via  $O_3 + NO = NO_2 + O_2$  (R1) and generated NO<sub>2</sub>. This conclusion is

also confirmed by Figure 3a, as shown in Figure 3a, NO<sub>2</sub> was first increased as NO decreased, which proved that R1 plays an important role in the process of NO oxidation. Higher nitrogen oxides were more difficult to form because there was not enough O<sub>3</sub> to react with NO<sub>2</sub>. For O<sub>3</sub>/NO, the concentration was 1, the experiment determined the NO concentration as 56 ppm and the simulation results of Model I and Model II were 48 ppm and 25 ppm, respectively. Hence, at T = 100 °C, the effect of the O<sub>3</sub> injection into NO was that O<sub>3</sub> could provide stronger oxidization help to transform NO into a higher oxidation state.

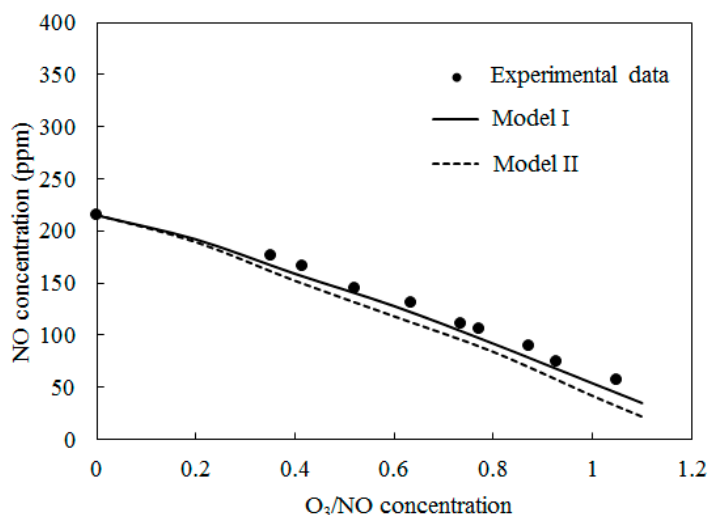


**Figure 4.** Variations of NO concentration with O<sub>3</sub>/NO concentrations at T = 100 °C.

Figure 5 depicts the comparisons of the computed NO concentration using Model I and Model II along with experimental data [27] at T = 200 °C. The O<sub>3</sub>/NO concentrations ranged from 0.0 to 1.1. A similar trend to Figure 4 was obtained.

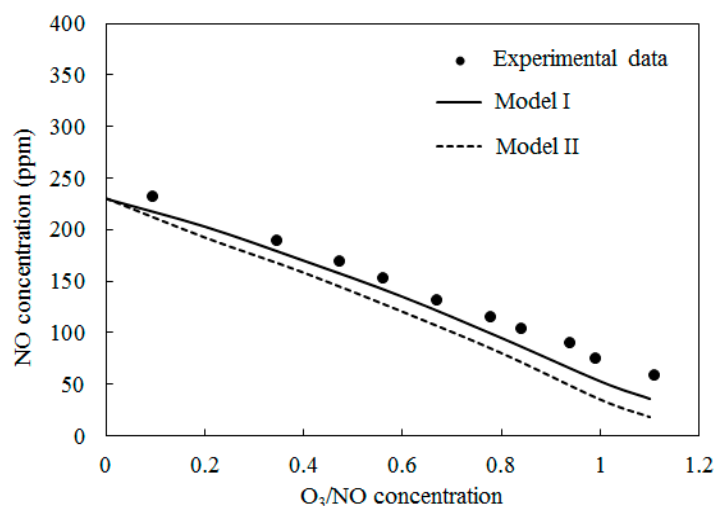


**Figure 5.** Variations of NO concentration with O<sub>3</sub>/NO concentrations at T = 200 °C.

The simulation results of both Model I and Model II under-predicted the experimental data. Where the O<sub>3</sub>/NO concentration equaled 1, the experiment determined NO concentration as 73 ppm; the simulation results of Model I and Model II were 53 ppm and 35 ppm, respectively.

Figure 6 shows the comparisons of computed NO concentration using Model I and Model II along with experimental data [27] at  $T = 300\text{ }^{\circ}\text{C}$ . The  $\text{O}_3/\text{NO}$  concentrations ranged from 0.0 to 1.1. The trends were similar to  $T = 100\text{ }^{\circ}\text{C}$  and  $T = 200\text{ }^{\circ}\text{C}$ . The NO concentration decreased as the  $\text{O}_3/\text{NO}$  concentrations increased. Where the  $\text{O}_3/\text{NO}$  concentrations equaled 1, the experiment determined the NO concentration as 124 ppm, and simulation results of Model I and Model II were 113 ppm and 93 ppm, respectively. Furthermore, compared with  $T = 100\text{ }^{\circ}\text{C}$  and  $T = 200\text{ }^{\circ}\text{C}$ , it was more difficult for NO to react with  $\text{O}_3$  at  $T = 300\text{ }^{\circ}\text{C}$ .

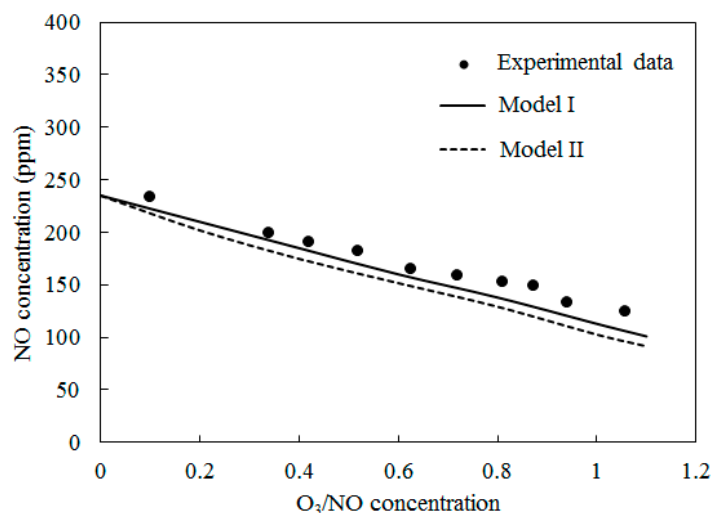


**Figure 6.** Variations of NO concentration with  $\text{O}_3/\text{NO}$  concentrations at  $T = 300\text{ }^{\circ}\text{C}$ .

In Figures 4–6, Model I shows closer agreement with experimental data compared with Model II. However, the two models exhibit the same prediction results in Figure 3 at lower temperature ( $T = 25\text{ }^{\circ}\text{C}$  and  $T = 40\text{ }^{\circ}\text{C}$ ). This result could be attributed to the differences of the reactions in the two models. At higher temperature, reaction  $\text{O}_3 = \text{O}_2 + \text{O}$  (R4) is more easy to be triggered and provides enough  $\text{O}_2$  for reaction  $\text{NO} + \text{NO} + \text{O}_2 = \text{NO}_2 + \text{NO}_2$  (R12) is responsible for consuming NO and generating  $\text{NO}_2$ , this reaction is included in Model II and it is not included in Model I. Therefore the NO concentration is slightly lower in prediction results of Model II compared with Model I in Figures 4–6.

To further discuss the effect of initial temperature on the NO conversion, Figure 7 shows the variations of NO conversion rate with temperatures  $T$  at  $\text{O}_3/\text{NO}$  concentration equals 1.0. The initial NO concentration and  $\text{O}_3$  concentration were kept at 300 ppm. The residence time was kept at 1 s. As shown in Figure 7, where temperatures were higher than  $200\text{ }^{\circ}\text{C}$ , the NO conversion rate was reduced sharply. At  $T = 300\text{ }^{\circ}\text{C}$ , the NO conversion rate is 48.5%. Previous studies [26,27] demonstrated that  $\text{O}_3$  becomes unstable at higher temperatures and decomposes to  $\text{O}_2$ . According to  $\text{O}_3 = \text{O}_2 + \text{O}$  (R4), NO will react with O through  $\text{NO} + \text{O} = \text{NO}_2$  (R6), which is more difficult trigger than R1. Therefore, a lesser amount of NO was transformed into  $\text{NO}_2$  at  $T = 300\text{ }^{\circ}\text{C}$ . The  $\text{O}_3$  decomposition at higher temperature leads to the decrease of NO conversion rate.

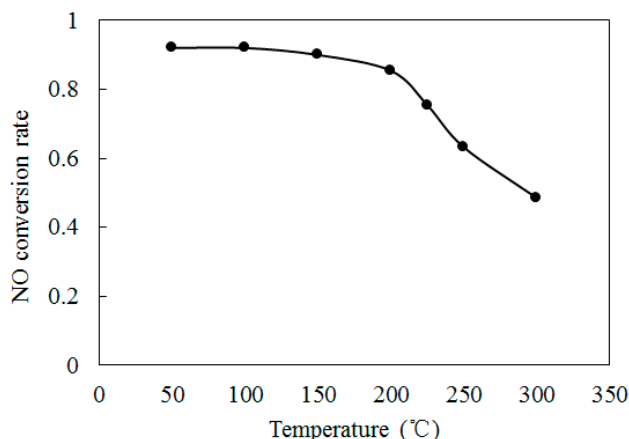


**Figure 7.** Variations of NO conversion rate with temperatures at O<sub>3</sub>/NO concentration equals 1.0.

In order to obtain further insight into the controlling chemical mechanism of the oxidation process, a sensitivity analysis of NO formation and NO<sub>2</sub> formation was conducted for comparison purposes. Figure 8 depicts the ranked logarithmic sensitivity coefficients of NO formation where the O<sub>3</sub>/NO concentration equaled 1.

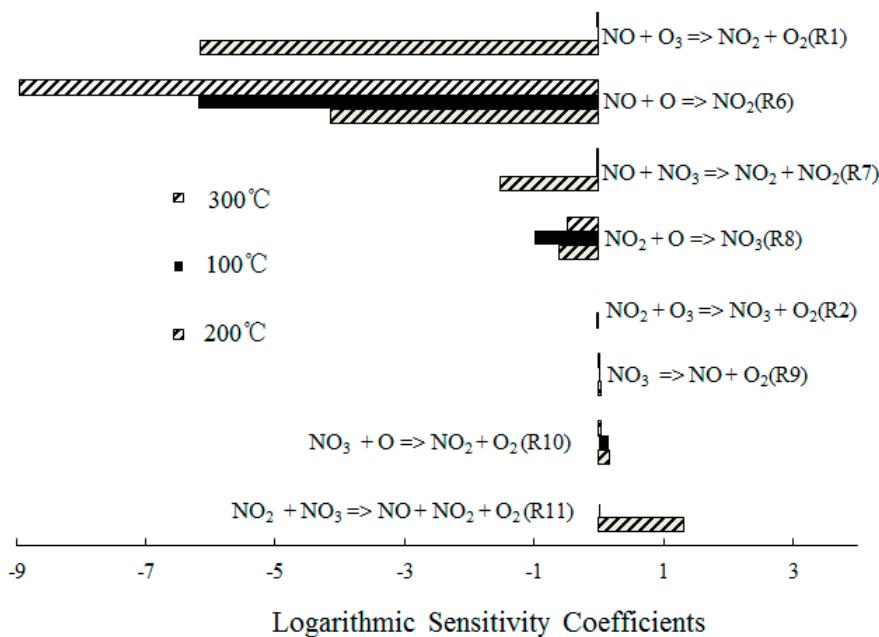


**Figure 8.** Ranked logarithmic sensitivity coefficients of NO formation where O<sub>3</sub>/NO concentration equals 1.

Reaction O<sub>3</sub> + NO = NO<sub>2</sub> + O<sub>2</sub> (R1) showed significant results at T = 100 °C, which indicated that the direct oxidation of NO by O<sub>3</sub> was the main reaction path of NO consumption. However, NO + O = NO<sub>2</sub> (R6) dominated the oxidation process of NO at T = 300 °C, which was expected for T = 300 °C; The O<sub>3</sub> decomposed to O<sub>2</sub> and O, a large amount of O was formed and then reacted with the excess NO. In addition, the reactions NO + NO<sub>3</sub> = NO<sub>2</sub> + NO<sub>2</sub> (R7) and NO<sub>2</sub> + O = NO<sub>3</sub> (R8) also showed significant results for the NO consumption. Hence, where a molar ratio of O<sub>3</sub>/NO equaled 1, a small amount of NO<sub>3</sub> was generated and reacted with NO.

Figure 9 depicts the ranked logarithmic sensitivity coefficients of NO<sub>2</sub> formation where the O<sub>3</sub>/NO concentration equaled 1. NO + NO<sub>3</sub> = NO<sub>2</sub> + NO<sub>2</sub> (R7) dominated the overall reactivity and also the NO<sub>2</sub>

formation at  $T = 300\text{ }^{\circ}\text{C}$ . At  $T = 200\text{ }^{\circ}\text{C}$ ,  $\text{NO} + \text{O}_3 = \text{NO}_2 + \text{O}_2$  (R1),  $\text{NO}_2 + \text{O}_3 = \text{NO}_3 + \text{O}_2$  (R2),  $\text{NO} + \text{O} = \text{NO}_2$  (R6) and  $\text{NO}_3 = \text{NO} + \text{O}_2$  (R9) had a positive effect on  $\text{NO}_2$  formation. The sensitivity coefficient of  $\text{NO} + \text{O}_3 = \text{NO}_2 + \text{O}_2$  (R1) was 0 at  $T = 300\text{ }^{\circ}\text{C}$ , which confirmed that  $\text{O}_3$  decomposed at  $T = 300\text{ }^{\circ}\text{C}$  [27]. There was insufficient  $\text{O}_3$  to react with  $\text{NO}$ ; therefore, the reaction  $\text{NO} + \text{O}_3 = \text{NO}_2 + \text{O}_2$  (R1) was subsequently difficult to trigger. Furthermore,  $\text{NO}_3 + \text{O} = \text{NO}_2 + \text{O}_2$  (R10) showed significant results in the  $\text{NO}_2$  formation due to a large amount of  $\text{O}$  formation.

Based on the previous discussion, the optimal reaction temperature for  $\text{O}_3/\text{NO}$  ranged from 100 to 200  $^{\circ}\text{C}$ . As the temperature increased,  $\text{O}_3$  decomposed into  $\text{O}$  and  $\text{O}_2$  before reacting with  $\text{NO}$ . The main oxidation reaction  $\text{NO} + \text{O}_3 = \text{NO}_2 + \text{O}_2$  (R1) of  $\text{NO}$  with  $\text{O}_3$  was difficult to trigger; therefore, the  $\text{NO}$  conversion rates were lower at  $T = 300\text{ }^{\circ}\text{C}$  compared with  $T = 100\text{ }^{\circ}\text{C}$  and  $T = 200\text{ }^{\circ}\text{C}$ . These conclusions indicate that in a coal-fired power plant, the  $\text{O}_3$  injection point should be set before or after the dust removal system, where the temperature of the flue gas is approximately 100~200 $^{\circ}\text{C}$ .

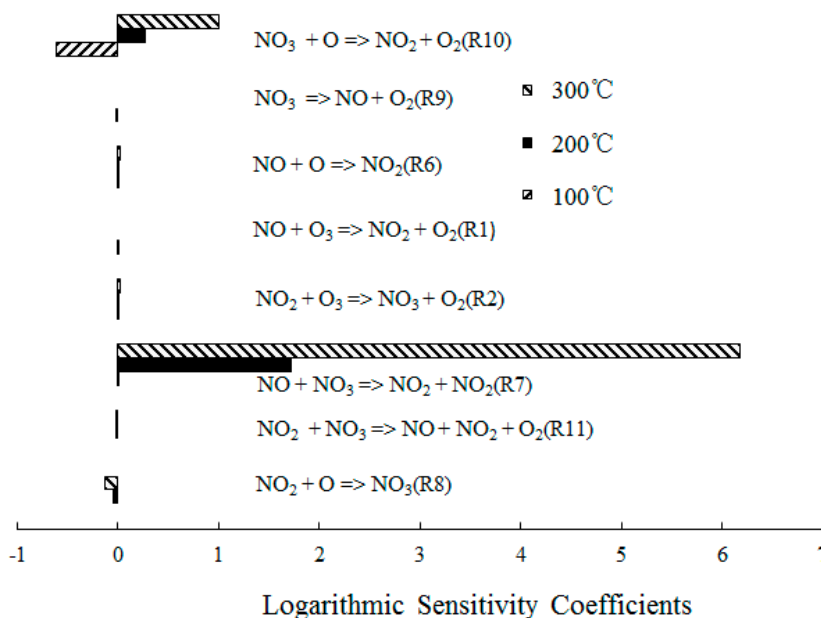


**Figure 9.** Ranked logarithmic sensitivity coefficients of  $\text{NO}_2$  formation where  $\text{O}_3/\text{NO}$  concentration equals 1.

The above discussions show that when the  $\text{O}_3/\text{NO}$  concentration was less than 1, most of the  $\text{NO}$  was oxidized into  $\text{NO}_2$ , and a higher oxidation state of  $\text{NO}_2$  was difficult produced due to insufficient  $\text{O}_3$ . For a further understanding of possible higher oxidative level  $\text{NO}_x$  species producing in the oxidation process at higher  $\text{O}_3/\text{NO}$  mole fraction ratios, the molar fraction variations of  $\text{NO}$ ,  $\text{NO}_2$ ,  $\text{NO}_3$  and  $\text{N}_2\text{O}_5$  for different temperatures where the  $\text{O}_3/\text{NO}$  concentration equaled 1.5 and 2.0 are discussed in Figures 10 and 11.

Figure 10 depicts the molar fraction variations of  $\text{NO}$ ,  $\text{NO}_2$ ,  $\text{NO}_3$  and  $\text{N}_2\text{O}_5$  for different temperatures where the  $\text{O}_3/\text{NO}$  concentration equaled 1.5 (with variable residence time). Figure 10a shows that at  $T = 100\text{ }^{\circ}\text{C}$ ,  $\text{NO}$  was first consumed, then  $\text{NO}_2$ ,  $\text{NO}_3$  and  $\text{N}_2\text{O}_5$  were generated. Figure 10b shows similar trends to Figure 10a for  $T = 200\text{ }^{\circ}\text{C}$ . Compared to an  $\text{O}_3/\text{NO}$  concentration equal to 1, a higher oxidation state of  $\text{NO}$  was produced where the  $\text{O}_3/\text{NO}$  concentration was higher than 1. The reactions R1, R2 and R12 are show significant importance at  $\text{O}_3/\text{NO}$  concentrations larger than 1.0,

which is also confirmed by previous studies [27,33]. At the beginning of the reaction, the NO oxidized to NO<sub>2</sub> by O<sub>3</sub> via reaction  $\text{NO} + \text{O}_3 = \text{NO}_2 + \text{O}_2$  (R1). As excess O<sub>3</sub> reacted with NO<sub>2</sub> via  $\text{NO}_2 + \text{O}_3 = \text{NO}_3 + \text{O}_2$  (R2), NO<sub>2</sub> rapidly decreased and NO<sub>3</sub> began to generate. N<sub>2</sub>O<sub>5</sub> was formed via reaction  $\text{NO}_2 + \text{NO}_3 = \text{N}_2\text{O}_5$  (R12). Hence, NO<sub>3</sub> and N<sub>2</sub>O<sub>5</sub> have a higher oxidization state than NO and they can be generated where there is an excess of O<sub>3</sub>. As demonstrated by previous study [25], reaction R2 was much slower than reaction R1, thus the NO<sub>3</sub> concentration was lower than NO<sub>2</sub> concentration. In addition, the N<sub>2</sub>O<sub>5</sub> produced by R12 decomposed into NO<sub>2</sub> and NO<sub>3</sub> by its reverse reaction, thus, the N<sub>2</sub>O<sub>5</sub> concentration was very low compared with NO<sub>2</sub> and NO<sub>3</sub>. Additionally, compared with T = 100 °C, the NO<sub>3</sub> mole fractions were higher at T = 200 °C, whereas the N<sub>2</sub>O<sub>5</sub> mole fractions were lower, this trend was also confirmed by calculated results from Mok *et al.* [25], indicating that at higher temperature, N<sub>2</sub>O<sub>5</sub> is more easy to be consumed by the reverse reaction of  $\text{NO}_2 + \text{NO}_3 = \text{N}_2\text{O}_5$  (R12).

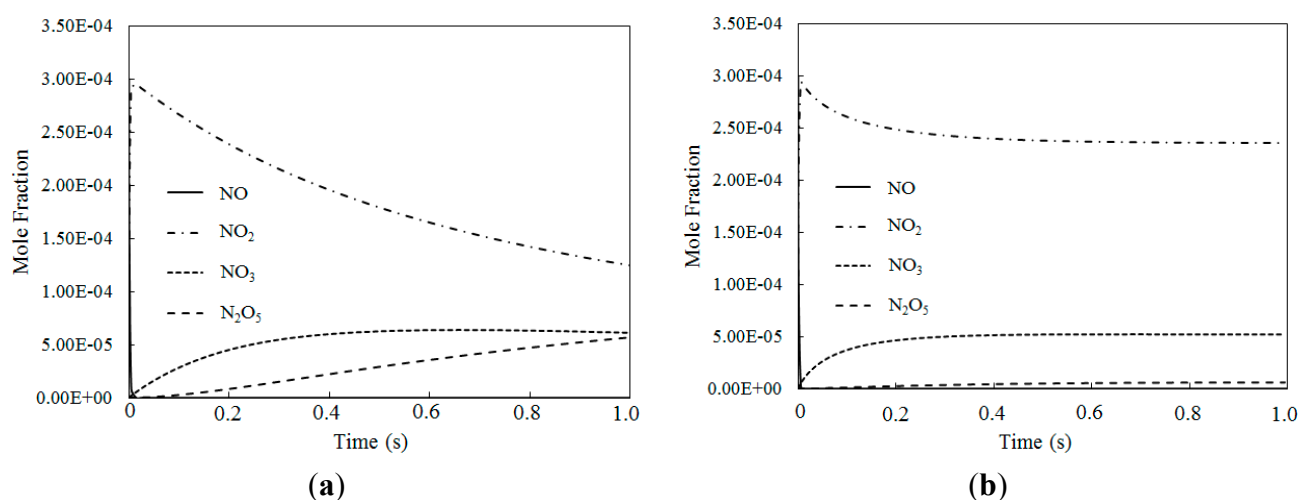


**Figure 10.** The mole fraction variations for NO, NO<sub>2</sub>, NO<sub>3</sub> and N<sub>2</sub>O<sub>5</sub> of different temperatures where O<sub>3</sub>/NO concentrations equal 1.5 for T = 100 °C and T = 200 °C. (a) T = 100 °C; (b) T = 200 °C.

Figure 11 depicts the mole fraction variations of NO, NO<sub>2</sub>, NO<sub>3</sub> and N<sub>2</sub>O<sub>5</sub> for different temperatures where the O<sub>3</sub>/NO concentrations equaled 2.0 (with variable residence time). The NO<sub>2</sub> mole fraction was nearly identical where the O<sub>3</sub>/NO concentrations equaled 1.5 and 2.0. However, where the O<sub>3</sub>/NO concentrations equaled 2, the NO<sub>3</sub> mole fraction was higher than when the O<sub>3</sub>/NO concentration equaled 1.5, which indicated that the O<sub>3</sub>/NO concentration had a significant effect on the mole fractions of the nitrogen oxidized products.

Figures 10 and 11 show that when the O<sub>3</sub>/NO concentration was greater than 1, higher oxidized products were formed (such as NO<sub>3</sub>, N<sub>2</sub>O<sub>5</sub>). NO<sub>2</sub> was first oxidized to produce NO<sub>3</sub> by the excess of O<sub>3</sub>, and then NO<sub>3</sub> reacted with NO<sub>2</sub> to produce N<sub>2</sub>O<sub>5</sub>, obtaining a higher oxidized state of NO.

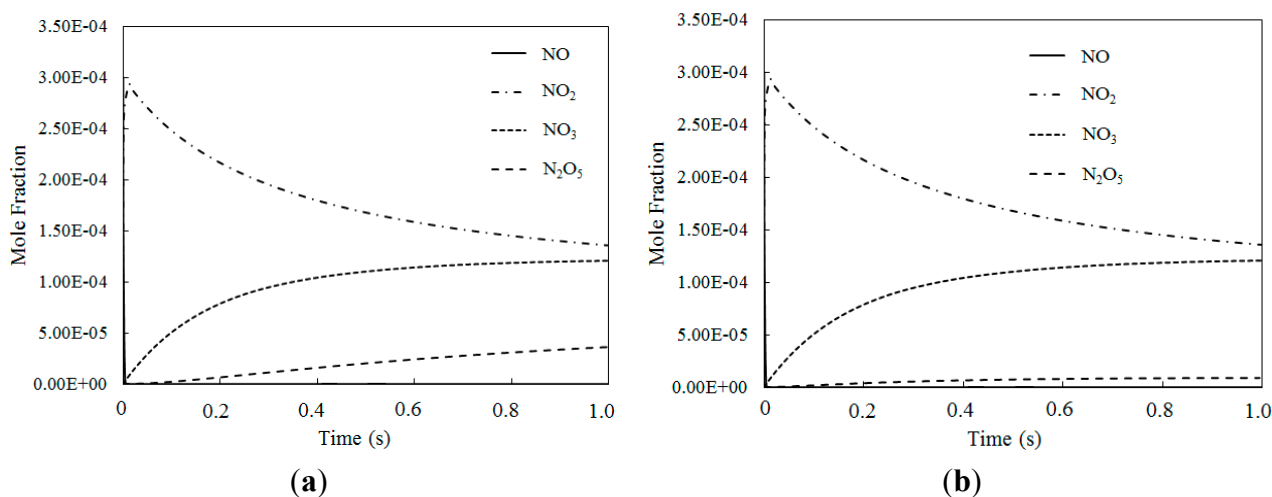


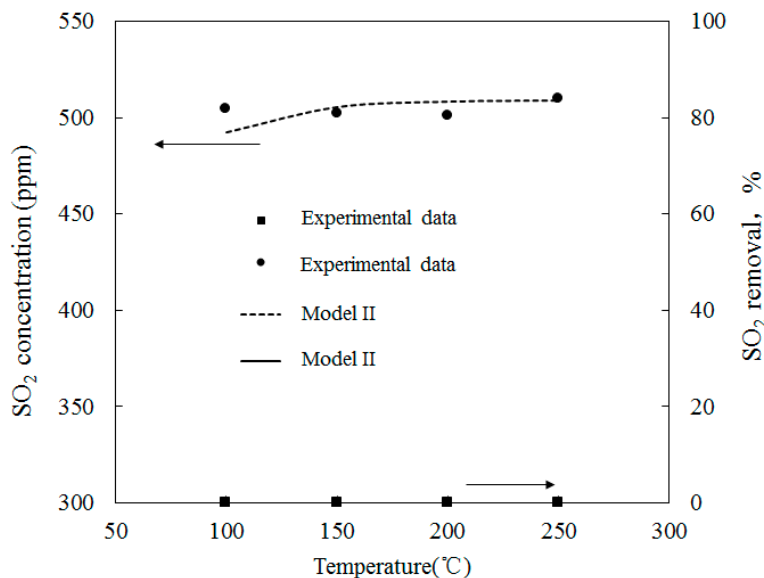
**Figure 11.** The mole fraction variations of NO, NO<sub>2</sub>, NO<sub>3</sub> and N<sub>2</sub>O<sub>5</sub> at different temperatures where O<sub>3</sub>/NO concentration equals 2 for T = 100 °C and T = 200 °C. (a) T = 100 °C; (b) T = 200 °C.

Simulation results for reaction products where the O<sub>3</sub>/NO concentrations were greater than 1 yielded clear evidence that NO could be oxidized to higher state oxidations such as NO<sub>3</sub> and N<sub>2</sub>O<sub>5</sub> by O<sub>3</sub> with appropriate O<sub>3</sub>/NO concentrations. Additionally, the results confirmed that Model I and Model II could both be used in modelling the experimental data or in predicting the effect of ozone injection into flue gas in practical applications. Finally, to ensure that all NO is transformed into a high oxidation state (such as NO<sub>2</sub>, NO<sub>3</sub> and N<sub>2</sub>O<sub>5</sub>), molar ratios where O<sub>3</sub>/NO is greater than 1 should be taken into account for practical applications.

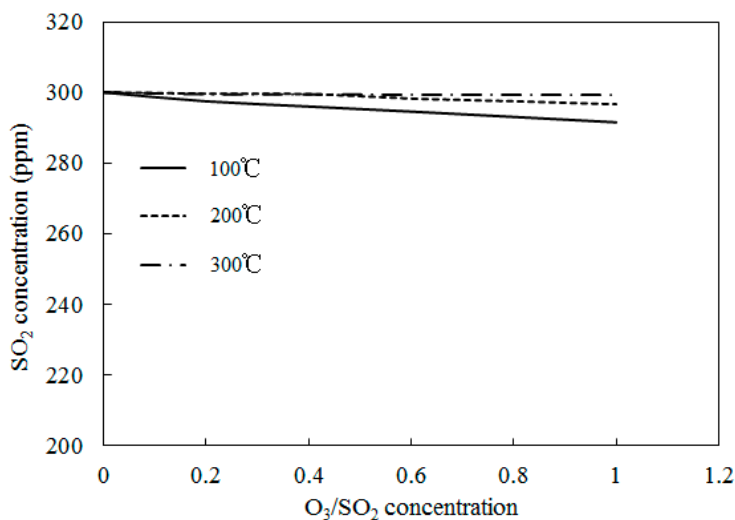
#### 4.3. SO<sub>2</sub> Oxidation by O<sub>3</sub>

Figure 12 depicts the variations of SO<sub>2</sub> concentrations with temperatures where the molar ratio of O<sub>3</sub>/SO<sub>2</sub> was equal to 1; SO<sub>2</sub> reduction rates are also shown. Experimental data provided by Wang [28], along with the simulation results of Model II, are also provided. The initial SO<sub>2</sub> concentration feeding into the reactor was 500 ppm and the temperature ranged from 100 to 250 °C. Figure 12 also shows that the temperature variations had little effect on the SO<sub>2</sub> mole concentration.

Simulations on the effect of the molar ratio of O<sub>3</sub>/SO<sub>2</sub> on variations of SO<sub>2</sub> concentrations were performed in order to obtain further insight into the interactions between O<sub>3</sub> and SO<sub>2</sub>. Figure 13 depicts the variations of SO<sub>2</sub> concentrations with O<sub>3</sub>/SO<sub>2</sub> mole fractions at different temperatures. The O<sub>3</sub>/SO<sub>2</sub> mole fractions ranged from 0 to 1.0. Simulations were performed with Model II. As discussed in Wang [28], Model I also demonstrated similar trends (not presented in the current study). Figure 12 shows that it was difficult for O<sub>3</sub> to oxidize SO<sub>2</sub> at various molar ratios of O<sub>3</sub>/SO<sub>2</sub>. Additionally, at lower temperatures (T = 100 °C), 10 ppm SO<sub>2</sub> could be transformed into SO<sub>3</sub> where the mole ratio of O<sub>3</sub>/SO<sub>2</sub> equaled 1; however, it appeared that the injection of ozone still had little effect on the oxidation of SO<sub>2</sub>. This may be caused by the reaction O<sub>3</sub> + SO<sub>2</sub> = O<sub>2</sub> + SO<sub>3</sub> (R1), which is the first step for SO<sub>2</sub> oxidation, had a large energy barrier in both Model I (13,910) and Model II (13,923). As such, it was difficult to trigger this reaction and, therefore, it was difficult for SO<sub>2</sub> to be oxidized.



**Figure 12.** Variations of SO<sub>2</sub> concentration with temperatures where the mole ratio of O<sub>3</sub>/SO<sub>2</sub> equals.



**Figure 13.** Variations of SO<sub>2</sub> concentrations with O<sub>3</sub>/SO<sub>2</sub> mole fractions at different temperatures.

For the process of SO<sub>2</sub> oxidation by O<sub>3</sub>, the results of both experiments and simulations indicated that SO<sub>2</sub> was not significantly oxidized and that variations of reaction temperatures and O<sub>3</sub>/SO<sub>2</sub> mole fractions had little effect on the SO<sub>2</sub> reduction. The appearance of SO<sub>2</sub> in the flue gas did not consume a large amount of O<sub>3</sub>.

#### 4.4. Simultaneous Oxidation of NO and SO<sub>2</sub> by O<sub>3</sub>

In the flue gas of a coal-fired power plant, large amounts of NO and SO<sub>2</sub> are mixed; therefore, the interactions between SO<sub>2</sub> and NO should be taken into account for practical applications of O<sub>3</sub> injection. Simulations of Model I and Model II, where the O<sub>3</sub>/NO/SO<sub>2</sub> mole fraction was 2:1:1, were conducted at different temperatures ranging from 100 to 250 °C. The results show that the appearance of NO did not promote the oxidation of SO<sub>2</sub> by O<sub>3</sub> and that the conversion of SO<sub>2</sub> was difficult. Furthermore, the NO conversion rate was not affected by the addition of SO<sub>2</sub>, which shows that SO<sub>2</sub> had little effect on the

oxidation of NO in the simultaneous oxidation of NO and SO<sub>2</sub> by ozone injection. This conclusion was also confirmed by Sun *et al.* [21] with situ IR measurements. Therefore, with respect to actual applications, O<sub>3</sub> injections could help NO transform into NO<sub>2</sub>, NO<sub>3</sub> and N<sub>2</sub>O<sub>5</sub>, which can then be absorbed in the scrubbing tower of the subsequent process with alkaline solution. Almost all of the SO<sub>2</sub> will be absorbed with the alkaline solution because it is difficult for SO<sub>2</sub> to be oxidized by the O<sub>3</sub> injection. Therefore, a scrubbing tower should be applied in order to achieve the simultaneous removal of NO and SO<sub>2</sub>.

## 5. Conclusions

This study used numerical simulations with two kinetic models to investigate the oxidation process of NO, SO<sub>2</sub> and NO/SO<sub>2</sub> mixtures by O<sub>3</sub>. The computed results were compared with experimental data from previous research. Two kinetic mechanisms were taken into account for modeling issues.

Both of the models showed satisfactory agreement with the experimental data with regards to NO oxidization by O<sub>3</sub>. The results showed that NO concentration decreased as the mole ratio of O<sub>3</sub>/NO increased (where the mole ratio of O<sub>3</sub>/NO was less than 1). NO<sub>2</sub> was the main product of the NO oxidation. The optimal reaction temperature for O<sub>3</sub>/NO ranged from 100 to 200 °C. As the temperature increased, O<sub>3</sub> easily decomposed to O and O<sub>2</sub> before reacting with NO. As such, the main oxidation reaction R1 of NO with O<sub>3</sub> was difficult to trigger. Therefore, the NO conversion rates were lower at T = 300 °C compared with T = 100 °C and T = 200 °C.

When the molar ratio of O<sub>3</sub>/NO was greater than 1, a higher oxidation state of NO (such as NO<sub>3</sub> and N<sub>2</sub>O<sub>5</sub>) was formed. Reaction NO<sub>3</sub> + O<sub>3</sub> = NO<sub>2</sub> + O<sub>2</sub> and reaction NO<sub>2</sub> + NO<sub>3</sub> = N<sub>2</sub>O<sub>5</sub> showed significant results in the oxidation process. First, NO<sub>2</sub> was generated; NO<sub>3</sub> was then produced by the oxidization of NO<sub>2</sub> and finally N<sub>2</sub>O<sub>5</sub> was produced by NO<sub>3</sub> reacting with NO<sub>2</sub>. Therefore, for practical applications, mole ratios of O<sub>3</sub>/NO greater than 1 are recommended in order to ensure that all NO is transformed into a high oxidation state (such as NO<sub>2</sub>, NO<sub>3</sub> and N<sub>2</sub>O<sub>5</sub>).

Both the experimental results and numerical simulation results showed that the oxidation of SO<sub>2</sub> was unaffected by injected ozone at different temperatures and mole ratios of O<sub>3</sub>/SO<sub>2</sub>. Computations of NO/SO<sub>2</sub>/O<sub>3</sub> showed that the NO conservation rate was not affected by the addition of SO<sub>2</sub> and that SO<sub>2</sub> had little effect on the oxidation of NO in the simultaneous oxidation of NO and SO<sub>2</sub> by the ozone injection. In summary, this study used two kinetic models for modeling the oxidation process of NO and SO<sub>2</sub> by O<sub>3</sub> injections. The optimized temperatures and mole ratios for NO/O<sub>3</sub> for further applications of O<sub>3</sub> injection for the control of pollutant emission in coal-fired power plants were suggested. Based on this study, a potentially viable facility for the simultaneous removal of NO, SO<sub>2</sub> and PM<sub>2.5</sub> was proposed.

## Author Contributions

Bo Li presented the original idea for the study. The study itself was conducted by Bo li and the co-authors. Bo Li carried out the simulations and analysis, and also drafted the manuscript, which was subsequently revised by all authors. All authors have read and approved the final manuscript.

## Conflicts of Interest

The authors declare no conflict of interest.

## References

1. Zhong, L.P.; Cao, Y.; Li, W.Y.; Pan, W.P.; Xie, K.C. Effect of the existing air pollutant control devices on mercury emission in coal-fired power plants. *J. Fuel Chem. Technol.* **2010**, *38*, 641–646.
2. Schopp, W.; Amann, M.; Cofala, J.; Heyes, C.; Klimont, Z. Integrated assessment of European air pollution emission control strategies. *Environ. Model. Softw.* **1999**, *14*, 1–9.
3. Schreifels, J.J.; Fu, Y.; Wilson, E.J. Sulfur dioxide control in China, policy evolution during the 10th and 11th Five-year Plans and lessons for the future. *Energy Policy* **2012**, *48*, 779–789.
4. Wang, F.; Du, Y.; Liu, Y.; Wang, X. The present development of flue gas denitrification technologies in domestic coal-fired power plants. *Electr. Power Environ. Prot.* **2007**, *23*, 20–23.
5. Song, X.; Yan, M. Influence factor analysis of the flue gas denitration of SCR design in the coal-fired power plant. *Saf. Environ. Eng.* **2013**, *20*, 68–71.
6. Bao, J.; Yang, L.; Song, S.; Xiong, G. Separation of fine particles from gassed in wet flue gas desulfurization system using a cascade of double tower. *Energy Fuel* **2012**, *26*, 2090–2097.
7. Ma, Y. The Selection of Flue Gas DeNO<sub>x</sub> Technology in the Power Plant of China. Master's Thesis, North China Electric Power University, Beijing, China, December 2005. (In Chinese)
8. Zhang, M.; Chen, J. The present situation and the development of the nitrogen oxides control in China's coal-fired power plant. *Sichuan Chem. Eng.* **2009**, *5*, 44–52. (In Chinese)
9. Carpenter, A.M. *Advances in Multi-Pollutant Control*; IEA: London, UK, 2013.
10. Yan, J.Y.; Zheng, Z.; Yu, G.F. Progress in study on multi-pollutant control technology for coal-fired flue gas. *Therm. Power Gener.* **2011**, *40*, 9–13.
11. Tavoulares, E.S.; Jozewicz, W. *Multi-Pollutant Emission Control Technology Options for Coal-Fired Power Plants*; EPA Report EPA-600/R-05/034; EPA: McLean, VA, USA, 2005.
12. Ghorishi, S.B.; Keeney, R.M.; Serre, S.D.; Gullett, B.K.; Jozewicz, W.S. Development of a Cl-impregnated activated carbon for entrained-flow capture of element mercury. *Environ. Sci. Technol.* **2002**, *36*, 4454–4459.
13. Callen, M.S.; Cruz, M.T.; Marinov, S.; Murillo, R.; Stefanova, M.; Mastral, A.M. Flue gas cleaning in power stations by using electron beam technology influence on PAH emission. *Fuel Process. Technol.* **2007**, *88*, 251–258.
14. Zhao, Y. Experiments and reaction characteristics of liquid phased simultaneous removal of SO<sub>2</sub> and NO. *Sci. China* **2009**, *52*, 1768–1775.
15. Jin, D.S.; Deshwal, B.R.; Park, Y.S.; Lee, H.K. Simultaneous removal of SO<sub>2</sub> and NO by wet scrubbing using aqueous chlorine dioxide solution. *J. Hazard. Mater.* **2006**, *135*, 412–417.
16. Yang, C.L. Aqueous absorption of nitric oxide induced by sodium chlorite oxidation in the presence of sulphur dioxide. *Environ. Prog.* **1998**, *17*, 80–85.
17. Liu, Y.; Zhang, J.; Sheng, C. Kinetic model of NO removal from SO<sub>2</sub>-containing simulated flue gas by wet UV/H<sub>2</sub>O<sub>2</sub> advanced oxidation process. *J. Chem. Eng.* **2011**, *168*, 183–189.

18. Sun, W.Y.; Ding S.L.; Zeng S.S.; Su, S.; Jiang W. Simultaneous absorption of NO<sub>x</sub> and SO<sub>2</sub> from flue gas with pyrolusite slurry combined with gas-phase oxidation of NO using ozone. *J. Hazard. Mater.* **2011**, *192*, 124–130.
19. Wei, L.S.; Zhou, J.H.; Wang Z.H.; Cen, K.F. Kinetic modelling of homogeneous low temperature multi-pollutant oxidation by ozone, the importance of SO and HCl in predicting oxidation. *J. Zhejiang Uni. Sci. A* **2006**, *7*, 335–339.
20. Wang, Z.H.; Zhou, J.; Zhu, Y.; Wen, Z.; Liu, J.; Cen, K. Simultaneous removal of NO<sub>x</sub>, SO<sub>2</sub> and Hg in nitrogen flow in a narrow reactor by ozone injection, experimental results. *Fuel Process. Technol.* **2007**, *88*, 817–823.
21. Sun, C.; Zhao, N.; Zhuang, Z.K.; Wang, H.; Liu, Y.; Weng, X.; Wu, Z. Mechanisms and reaction pathways for simultaneous oxidation of NO<sub>x</sub> and SO<sub>2</sub> by ozone determined by *in situ* IR measurements. *J. Hazard. Mater.* **2014**, *274*, 376–383.
22. Skalska, K.; Miller, J.S.; Ledakowicz, S. Intensification of NO<sub>x</sub> absorption process by means of ozone injection into exhaust gas stream. *Chem. Eng. Process. Process Intensif.* **2012**, *61*, 69–74.
23. Mok, Y.S. Absorption-reduction technique assisted by ozone injection and sodium sulfide for NO<sub>x</sub> removal from exhaust gas. *Chem. Eng. J.* **2006**, *118*, 63–67.
24. Sun, W.; Wang, Q.Y.; Ding, S.L.; Su, S. Simultaneous absorption of SO<sub>2</sub> and NO<sub>x</sub> with pyrolusite slurry combined with gas-phase oxidation of NO using ozone, Effect of molar ratio of O<sub>2</sub>/(SO<sub>2</sub> + 0.5 NO<sub>x</sub>) in flue gas. *Chem. Eng. J.* **2013**, *228*, 700–707.
25. Stamate, E.; Chen, W.; Jorgensen, L.; Jensen, T.K.; Fateev, A.; Michelsen, P.K. IR and UV gas absorption measurements during NO<sub>x</sub> reduction on an industrial nature gas fired power plant. *Fuel* **2010**, *89*, 978–985.
26. Mok, Y.S.; Lee, H.J. Removal of sulfur dioxide and nitrogen oxides by using ozone injection and absorption-reduction technique. *Fuel Process. Technol.* **2006**, *87*, 591–597.
27. Wang, Z.H. Mechanism Study on Multi-Pollution Control Simultaneously during Coal Combustion and Direct Numerical Simulation of Reaction Jet Flow. Ph.D. Thesis, Zhejiang University, Hangzhou, China, 2005. (In Chinese)
28. Wang, J. The Experimental Study of Oxidative-Desulfurization in the O<sub>3</sub> Multi-Pollutant Control Technology. Master's Thesis, Zhejiang University, Hangzhou, China, 2008. (In Chinese)
29. Wen, Z.C. Mechanism Investigation on the Oxidation and Degradation of Multiple Pollutants in Flue Gas by Ozone. Ph.D. Thesis, Zhejiang University, Hangzhou, China, 2009. (In Chinese)
30. Leeds NO<sub>x</sub> & SO<sub>2</sub> Mechanism. Available online: <http://garfield.chem.elte.hu/combustion/nox.htm> (accessed on 17 December 2014).
31. Kee, R.J.; Rupley, F.M.; Miller, J.A. *Chemkin II: A Fortran Chemical Kinetics Package for the analysis of Gas-Phase Chemical Kinetics*; Sandia Report, SAND 89-8009; Sandia National Laboratories: Livermore, CA, USA, 1989.
32. Mallard, W.G.; Westley, F.; Herron, J.T.; Hampson, R.F.; Frizzell, D.H. *NIST Chemical Kinetics Database*; NIST: Gaithersburg, MD, USA, 1998.

33. Skalska, K.; Miller, J.S.; Wilk, M.; Ledakowicz, S. Nitrogen oxidizes ozonation as a method for NO<sub>x</sub> emission abatement. *Ozone Sci. Eng.* **2012**, *34*, 252–258.

© 2015 by the authors; licensee MDPI, Basel, Switzerland. This article is an open access article distributed under the terms and conditions of the Creative Commons Attribution license (<http://creativecommons.org/licenses/by/4.0/>).